Available online at www.sciencedirect.com

ScienceDirect

Ceramics International 40 (2014) 1569–1574

CERAMICS INTERNATIONAL

www.elsevier.com/locate/ceramint

Sol–gel synthesis and dielectric properties of Ruddlesden–Popper phase $Sr_{n+1}Ti_nO_{3n+1}$ ($n=1, 2, 3, \infty$)

Wenwen Ge, Chunhui Zhu, Heping An, Zhuangzhi Li*, Guide Tang, Denglu Hou

Hebei Advanced Thin Films Laboratory, Department of Physics, Hebei Normal University, Shijiazhuang City 050024, People's Republic of China

Received 14 April 2013; received in revised form 7 July 2013; accepted 7 July 2013
Available online 16 July 2013

Abstract

A series of high purity Ruddlesden–Popper phase $Sr_{n+1}Ti_nO_{3n+1}$ ($n=1, 2, 3, \infty$) nanoscale powders have been produced by the sol–gel method. The final sintering temperatures of $SrTiO_3$, $Sr_4Ti_3O_{10}$, $Sr_3Ti_2O_7$ and Sr_2TiO_4 determined by TG-DSC analysis were 800 °C, 950 °C, 1050 °C and 1050 °C, respectively. The single phase structures of the four powders were identified by X-ray diffraction analysis. The different molecular structures and the different vibration bands were studied by Fourier transform infrared absorption spectroscopy and Raman spectroscopy. The dielectric constants of $SrTiO_3$, $Sr_4Ti_3O_{10}$, $Sr_3Ti_2O_7$ and Sr_2TiO_4 were measured to be 114, 55, 41 and 30, respectively, at 100 kHz. The dielectric losses of the four materials were found to be lower than 4×10^{-2} above 100 kHz.

Keywords: A. Sol–gel; C. Dielectric properties; $Sr_{n+1}Ti_nO_{3n+1}$; Nanoscale powders

1. Introduction

ABO_3-type perovskite composite oxides are important inorganic compounds and are versatile functional materials. Among the perovskite compounds, $SrTiO_3$ is an important material for electronics because it has the advantages of high dielectric constant, low dielectric loss and good thermal stability. It is widely used to make a variety of components including degaussed components, self-regulating heating elements, ceramic sensors and microwave ceramic components [1]. In particular, high quality $SrTiO_3$ powder can be used to produce boundary layer capacitors and PTC thermistor components, which have high performance, high reliability and small size. Furthermore, $SrTiO_3$ powder can also be used to make paints, enamel, insulation and heat-resistant materials. Currently, $SrTiO_3$ powder is also used as a catalyst for soot combustion [2].

Since $SrTiO_3$ is a member of the $Sr_{n+1}Ti_nO_{3n+1}$ Ruddlesden–Popper (R–P) homologous series with $n=\infty$ [3,4], it is of interest to expand the investigation of $SrTiO_3$ powder to other members of the $Sr_{n+1}Ti_nO_{3n+1}$ R–P phase powders. The $Sr_{n+1}Ti_nO_{3n+1}$ R–P phases have a cubic layered perovskite structure consisting of SrO layers and TiO_2 layers alternatively stacked [5]. In this paper, we focus on the R–P phases for which the molecular formula is $Sr_{n+1}Ti_nO_{3n+1}$ ($n=1, 2, 3, \infty$). For $n=1$, the molecular formula is Sr_2TiO_4[($SrTiO_3$)SrO]. It has a square structure which consists of a set of two layers of SrO followed by one layer of TiO_2. For $n=2$, the molecular formula is $Sr_3Ti_2O_7$[($SrTiO_3$)$_2$SrO]. It has a square structure which consists of a set of three layers of SrO followed by two layers of TiO_2. For $n=3$, the molecular formula is $Sr_4Ti_3O_{10}$[($SrTiO_3$)$_3$SrO]. It has a square structure which consists of a set of four layers of SrO followed by three layers of TiO_2. For $n=\infty$, the molecular formula is $SrTiO_3$, which consists of single SrO and TiO_2 layers alternatively stacked.

The methods of producing $SrTiO_3$ powder are mainly based on solid state reactions, chemical precipitation and the sol–gel method. At present, the sol–gel method is the center of attention due to its many advantages, such as a high purity product, excellent uniformity and low sintering temperatures. In 1993, Pfaff et al. synthesized R–P phase $Sr_{n+1}Ti_nO_{3n+1}$ ($n=1, 2, 3, \infty$) using the sol–gel method with raw materials of strontium acetate and titanium isopropoxide [6]. However, compared to the flash point of 22 °C for titanium isopropoxide, which was the titanium source,

*Corresponding author. Tel.: +86 311 80787330.
E-mail address: zzli@mail.hebtu.edu.cn (Z. Li).

0272-8842/$ - see front matter © 2013 Elsevier Ltd and Techna Group S.r.l. All rights reserved.
http://dx.doi.org/10.1016/j.ceramint.2013.07.044

the value 77 °C for tetrabutyl titanate makes the latter much safer to use. In 2001, high purity, uniform $SrTiO_3$ ($n=\infty$) powder was produced by Wang et al. using a new sol–gel process with raw materials of strontium nitrate and tetrabutyl titanate [7], but they reported no similar work for the $n=1$, 2, 3 members of the $Sr_{n+1}Ti_nO_{3n+1}$ series.

Dielectric materials are of great value in the electronics industry, and the dielectric properties of R–P phase $Sr_{n+1}Ti_nO_{3n+1}$ have been studied by several groups. At an early stage, Sohn and collaborators synthesized R–P phase $Sr_{n+1}Ti_nO_{3n+1}$ powders using a solid state reaction and studied their dielectric properties [8]. The dielectric properties of epitaxial films of the R–P $Sr_{n+1}Ti_nO_{3n+1}$ series fabricated by molecular beam epitaxy (MBE) have also been measured [5,9]. However, these films exhibited oriented growth and could not show the average dielectric performance. On the other hand, considering that the grain size of powders produced by the sol–gel method is much smaller and more uniform than that of solid state reactions, it is necessary to investigate the dielectric properties of R–P phase $Sr_{n+1}Ti_nO_{3n+1}$ powders produced by the sol–gel method. To the best of our knowledge, among these powders synthesized by the sol–gel method, the dielectric properties of $SrTiO_3$ and Sr_2TiO_4 have been studied [10], but not for $Sr_3Ti_2O_7$ and $Sr_4Ti_3O_{10}$.

In the work reported here, Wang et al.'s process was utilized to synthesize $n=1$, 2, 3 R–P phase $Sr_{n+1}Ti_nO_{3n+1}$ powders, and $SrTiO_3$ with $n=\infty$ was also produced for comparison. The crystal structures and grain sizes of these powders were characterized by X-ray diffraction. The infrared absorption and Raman spectral response were measured to study the vibration and rotation modes. The relationship of the dielectric properties to the index n of the $Sr_{n+1}Ti_nO_{3n+1}$ series is discussed.

2. Experimental details

High purity $SrTiO_3$ powder was first produced using the sol–gel method by Wang et al. [7]. During the preparation, the raw materials were $Sr(NO_3)_2$ and $Ti(OC_4H_9)_4$, while the solvents were absolute ethyl alcohol and deionized water. Glacial acetic acid and HNO_3 were chosen as suppressants to prevent hydrolysis in the reaction process. Citric acid was chosen as the complexing agent for the gel. It should be noted that in the procedure outlined above, there are two points that differ from the aforementioned report by Wang et al. Firstly, we observed that glacial acetic acid together with nitric acid was more effective as a suppressant than just glacial acetic acid alone. The other point of difference is that citric acid was used as the complexing agent in this work.

The details of the fabrication of the $SrTiO_3$ powder are shown in Fig. 1. Firstly, 0.05 mol of $Sr(NO_3)_2$ was dissolved in deionized water, with constant stirring, until fully dissolved. A small quantity of HNO_3 was simultaneously added to the solution to give a nitric acid strontium solution referred to below as solution A. A second solution was made by adding 0.05 mol of $Ti(OC_4H_9)_4$ to a solution of 100 ml absolute ethyl alcohol and 10 ml glacial acetic acid. This solution is referred to below as solution B. Solution B was then added slowly to solution A with stirring until a transparent solution was obtained. Citric acid was then added to the solution and stirred until a uniform transparent sol was obtained. The sol was dried for 48 h in a water bath at 50 °C, and then was put into a drying box and further dried for 12 h at 220 °C to obtain a gel. The gel powder was pulverized and pre-sintered at 600 °C in air for 12 h to volatilize the organic materials and yields the $SrTiO_3$ precursor powder. The precursor powder was ground and then sintered at 800 °C for 12 h, followed by re-grinding. This yielded the $SrTiO_3$ powder.

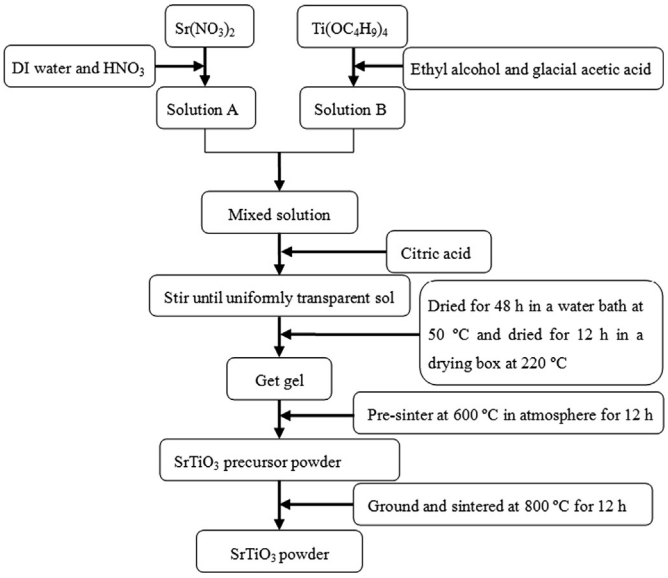

Fig. 1. Flow-process diagram for fabricating $SrTiO_3$ powder using sol–gel method.

By changing the stoichiometric ratios of solutions A and B and using the same process as described above, we produced Sr_2TiO_4, $Sr_3Ti_2O_7$ and $Sr_4Ti_3O_{10}$ precursor powders. Using a thermal analysis system (TGA7, PerkinElmer in the USA), we obtained the TG-DSC characteristic curves of the gel powders, which allowed the final sintering temperatures of the gel powers to be evaluated for R–P phase $Sr_{n+1}Ti_nO_{3n+1}$ ($n=1$, 2, 3, ∞). The phases of the powders and the grain sizes were investigated with X-ray diffraction (XRD, X'Pert Pro MRD, Cu k_α, PANalytical B. V. in the Netherlands). The molecular bond lengths and angles were characterized by Fourier transform infrared spectrum (FT-IR, Nicolet 380, Thermo in the USA). The vibration and rotation modes of the molecules were analyzed by Fourier transform Raman spectrum (VERTEX 70, Brook in Germany). The dielectric constants and dielectric losses were measured using a Precision Impedance Analyzer (4294A, Agilent in the USA). For the measurement of dielectric properties, the powders were pressed into pellets of diameter and thickness 30 mm and 1.0 mm, respectively, and sintered at 800 °C for 6 h. Thin silver paint layers were coated on the surfaces of the pellets as shown in the inset of Fig. 6(b) and baked at 140 °C for 15 min before measurement.

3. Results and discussions

3.1. Analysis of TG-DSC curves

Results for the TG-DSC measurement performed for Sr_2TiO_4 precursor powder are shown in Fig. 2 for the temperature range

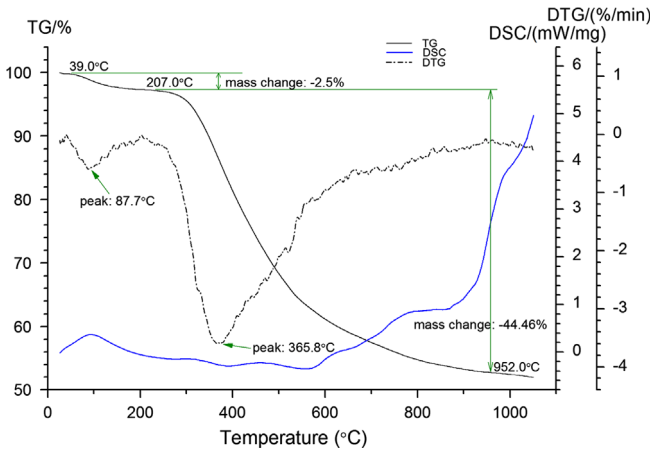

Fig. 2. TG-DSC curves for Sr_2TiO_4 sample powder.

30–1050 °C. $Sr_3Ti_2O_7$, $Sr_4Ti_3O_{10}$ and $SrTiO_3$ powders were also measured and similar results were obtained.

TG curves show the change in weight of a sample as the temperature increases. The weight loss of all the samples was significant, but the weight losses had different rates in different temperature ranges. Reduction of weight is the result of the evaporation of water and the decomposition of organics [7,11]. As shown in Fig. 2, from room temperature to 100 °C range, the reduction in weight is ascribed to the evaporation of water. After 100 °C the reduction of weight is mainly due to the decomposition of organics. DSC curves reflect the exothermic or endothermic behavior of the samples with the increase in temperature. An exothermic peak appeared in 100–400 °C range due to decomposition of a large number of organic compounds. The exothermic peak appearing in the 400–580 °C range was due to the decomposition of the remaining organics and NO_3^-. The endothermic peak appearing in the 600–900 °C range is due to the formation of the Sr_2TiO_4 phase. After 1000 °C, the TG curve changes little and shows no exothermic or endothermic peaks. With this analysis we obtained a preliminary estimate that the final sintering temperature of Sr_2TiO_4 powder is 1050 °C. This was verified by XRD analysis after calcining for 12 h at this temperature. The final sintering temperatures of $SrTiO_3$, $Sr_4Ti_3O_{10}$ and $Sr_3Ti_2O_7$, as determined from the corresponding TG-DSC curve analyses, are 800 °C, 950 °C and 1050 °C, respectively.

3.2. Phase analysis with XRD patterns

The crystallographic properties of different materials in the R–P phase were studied by XRD. Fig. 3 shows XRD patterns for the series of $Sr_{n+1}Ti_nO_{3n+1}$ ($n=1, 2, 3, \infty$) powders made by the sol–gel method. The four powders correspond to $SrTiO_3$ [01-086-0179], Sr_2TiO_4 [01-072-2040], $Sr_3Ti_2O_7$ [00-011-0663], and $Sr_4Ti_3O_{10}$ [01-076-0741] in the XRD PDF card library, respectively. There are no impurity peaks, which indicates that the four powders are pure single phase powders. As shown in Fig. 3, all four powders have (110) and (200) diffraction peaks, but Sr_2TiO_4, $Sr_3Ti_2O_7$ and $Sr_4Ti_3O_{10}$ powders show some differences with respect to the $SrTiO_3$ powder.

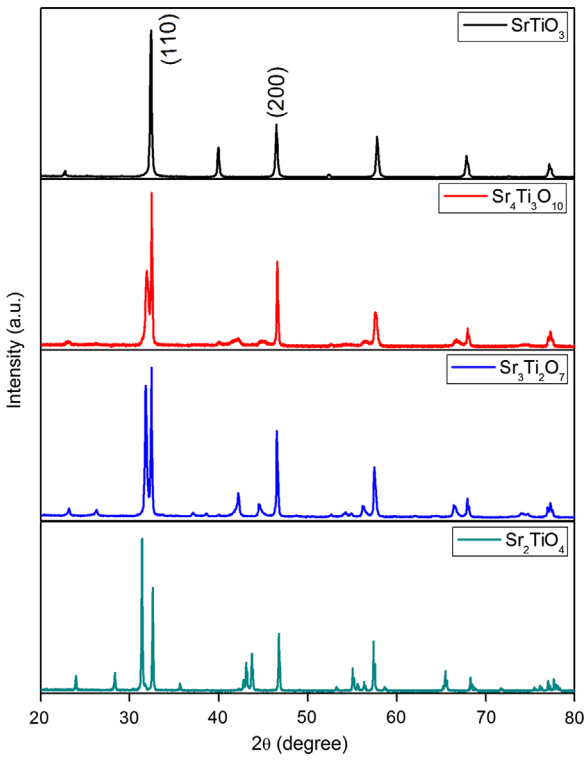

Fig. 3. XRD patterns for $Sr_{n+1}Ti_nO_{3n+1}$ ($n=1, 2, 3, \infty$) powders.

The (110) peak is the main peak for $SrTiO_3$, but not for Sr_2TiO_4, $Sr_3Ti_2O_7$ and $Sr_4Ti_3O_{10}$. The latter three powders show double peaks at this specific position, which gradually change to a single peak as the index n increases. The (200) peak shows no obvious change for the four powders, and the peak value is about one half the height of the (110) peak. It is evident that some peaks gradually disappear as n increases, and the XRD pattern becomes more and more similar to the $SrTiO_3$ pattern. The crystal system also changes as n increases, so that Sr_2TiO_4, $Sr_3Ti_2O_7$ and $Sr_4Ti_3O_{10}$ powders belong to the square crystal system, but $SrTiO_3$ powder belongs to the cubic crystal system.

The size of the grains in a powder can be obtained through the Scherrer formula $D=0.89\lambda/B\cos\theta$, where λ is the X-ray wavelength, θ is the Bragg angle, and B is the full width at half-maximum of the Bragg peak [11]. From the XRD patterns in Fig. 3, when n equals 1, 2, 3, ∞, the grain size can be evaluated to be about 350 nm, 100.5 nm, 88.8 nm and 86.7 nm, respectively.

3.3. Infrared absorption spectroscopy

Fig. 4 shows infrared absorption spectrums for the $Sr_{n+1}Ti_nO_{3n+1}$ ($n=1, 2, 3, \infty$) powders. The bond lengths and bond angles of the molecules were measured using FT-IR, and the spatial configuration of the molecules can be inferred from the results. The large number of infrared absorption peaks appearing in the spectrum is due to the large number of atoms in the $Sr_{n+1}Ti_nO_{3n+1}$ ($n=1, 2, 3, \infty$) unit cells. Each peak corresponds to a vibration. According to Kamba et al.'s report

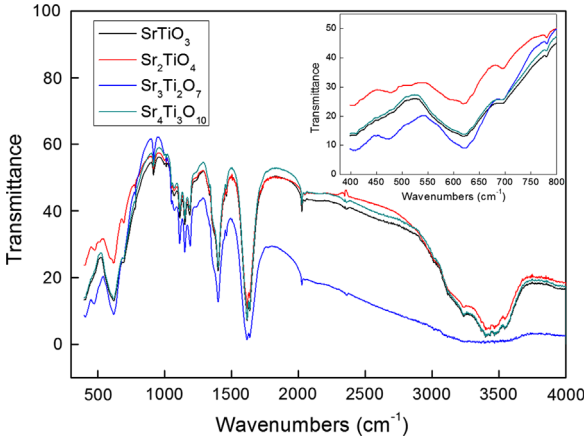

Fig. 4. Infrared absorption spectrums for $Sr_{n+1}Ti_nO_{3n+1}$ ($n=1, 2, 3, \infty$) powders. The inset is a magnification for the wavenumber range 400–800 cm^{-1}.

[12], the vibrations of $Sr_{n+1}Ti_nO_{3n+1}$ ($n=1, 2, 3, \infty$) can be divided into 4 modes. The first mode (TO_1) is consistent with octahedral elastic vibrations (interaction between Ti and O). The second mode (TO_2) is a translational vibration (Sr against the TiO_6 octahedron). The third mode (TO_3) relates to rotations of oxygen and is silent. These peaks are unclear in the current spectrum. The fourth mode (TO_4) is a bending vibration of oxygen [13]. Only TO_4 can be found in Fig. 4 due to the fact that the wavenumber range measured covered only 400–4000 cm^{-1}. For Sr_2TiO_4, TO_4 peaks appear at 510.0 cm^{-1}, 547.0 cm^{-1} and 701.5 cm^{-1}. For $Sr_3Ti_2O_7$, they appear at 515.0 cm^{-1}, 541.8 cm^{-1} and 697.1 cm^{-1}. For $Sr_4Ti_3O_{10}$, they appear at 518.7 cm^{-1}, 543.7 cm^{-1} and 704.7 cm^{-1}. For $SrTiO_3$, the TO_4 vibration appears only at 548.0 cm^{-1}. The simultaneous existence of the three wavenumbers for $Sr_{n+1}Ti_nO_{3n+1}$ ($n=1, 2, 3$) is caused by the coupling between O–O atoms in these cells [13]. The absorption peak at 550 cm^{-1} possibly contains contributions from vibrations of Ti–O and Sr–O bonds besides the TO_4 peaks [14]. The absorption peaks appearing at or near 850 cm^{-1} and 1500 cm^{-1} are attributed to $SrCO_3$. The appearance of CO_3^{2-} is due to CO_2 and H_2O in air. The telescopic vibration of OH^- which appears at 3500 cm^{-1} is attributed to water vapor adsorbed on the sample surfaces. The varying intensity of the peaks is proportional to the square of the dipole moment of the molecular vibrations. This means that the greater the difference in symmetry, the greater the infrared absorption. The inset of Fig. 4 is a magnification of the wavenumber range 400–800 cm^{-1}. As shown in the illustration, the four spectrums exhibit some differences in the range 400–475 cm^{-1}. Compared with the spectrum for the $SrTiO_3$ powder, an extra peak appears for Sr_2TiO_4 and $Sr_3Ti_2O_7$ powders at about 440 cm^{-1}. However, the $Sr_4Ti_3O_{10}$ powder has no peak at this wavenumber. Group theory indicates that the peak in the range 400–475 cm^{-1} corresponds to 1st order scattering for Sr_2TiO_4 and $Sr_3Ti_2O_7$ and that no 1st order scattering peak for $Sr_4Ti_3O_{10}$ and $SrTiO_3$ should appear in this range [12]. As can be seen, as the index n increases, the FT-IR curve for $Sr_{n+1}Ti_nO_{3n+1}$ becomes more and more similar to that for $SrTiO_3$, with the result that the infrared spectrum of $SrTiO_3$ powder and $Sr_4Ti_3O_{10}$ powder are almost coincident.

3.4. Raman spectrum analysis

Fig. 5 shows the Fourier transform Raman spectrum for the $Sr_{n+1}Ti_nO_{3n+1}$ ($n=1, 2, 3, \infty$) series of powders. The number of spectral lines, the size of the displacement and the width of the spectral lines are directly related to molecular vibrations or rotational levels. Therefore, Raman spectrum analysis is similar to infrared absorption spectroscopy as it gives information about molecular vibrations or rotations. Among the $Sr_{n+1}Ti_nO_{3n+1}$ ($n\leq3$) samples, many Raman peaks are stronger than those observed in the $SrTiO_3$ sample. This phenomenon is caused by the highly symmetrical cubic structure of $SrTiO_3$.

Some peaks may be ascribed to multiphonon scattering and absorption [15–17]. From the XRD patterns of the four powders, it can be seen that the powders belong to different crystal systems, but many of the same peaks appear in XRD. This may be due to a nonperiodic stacking sequence along the *c*-axis [5]. These stacking fault structures activate phonons outside the center of the Brillouin zone [12]. For instance, Raman peaks appearing below 150 cm^{-1} may well indicate the

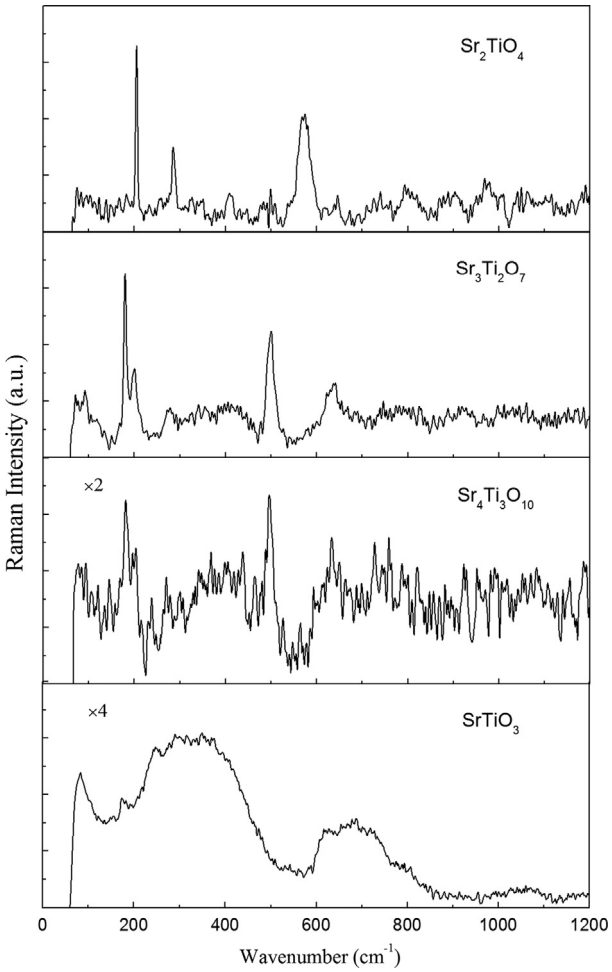

Fig. 5. Fourier transform Raman spectrum for $Sr_{n+1}Ti_nO_{3n+1}$ ($n=1, 2, 3, \infty$) powders.

activation of the acoustic mode, due to the folded structure of the Brillouin zone. The other peaks that appear are the result of double-phonon scattering [18]. As may be seen from Fig. 5, $SrTiO_3$ and $Sr_4Ti_3O_{10}$ powders have the same constituent elements, but the different compositions lead to different structures.

3.5. Dielectric constant and dielectric loss analysis

Fig. 6(a) shows the frequency dependence of the dielectric constant for the $Sr_{n+1}Ti_nO_{3n+1}$ ($n=1, 2, 3, \infty$) samples. It can be seen that the magnitude of the dielectric constant shows only small changes in the 1 kHz to 10 MHz range. The dielectric constant is a physical quantity which usually describes the polarization and stored charge capacity of a material. The dielectric constant represents the degree of polarization for a dielectric material. In other words, it represents the ability to bind charges. This means that a larger ability to bind charge leads to a larger dielectric constant hence better insulation [1,19]. Electronic polarization is present in all types of solid state substances. Besides the nature of the material itself, the dielectric constant is also affected by the temperature and electric field frequency. In Fig. 6(a), the four samples were tested at the same temperature. The dependence on frequency of the dielectric constants for the four materials is approximately the same, but it may be seen that the dielectric constant increases with n. At 100 kHz, for instance, the values of the dielectric constants for $SrTiO_3$, $Sr_4Ti_3O_{10}$, $Sr_3Ti_2O_7$ and Sr_2TiO_4 are 114, 55, 41 and 30, respectively. This means that the dielectric constants of the four materials vary regularly with their crystal structures, i.e., the values increase with the number of sub layers in the structures. An earlier report on the dielectric constants of $SrTiO_3$ and Sr_2TiO_4 prepared by the sol–gel method gave 90 and 30 respectively [10], which is similar to our results. Wise et al. have synthesized R–P phase $Sr_{n+1}Ti_nO_{3n+1}$ powders using solid state reactions. In their report, the microwave dielectric constants of $SrTiO_3$, $Sr_4Ti_3O_{10}$, $Sr_3Ti_2O_7$ and Sr_2TiO_4 were 190, 76.1, 57.9 and 37.4, respectively [20]. These results are slightly larger than our results, but show a similar trend as n increases. Orloff et al. have synthesized $Sr_4Ti_3O_{10}$, $Sr_3Ti_2O_7$ and Sr_2TiO_4 using MBE, and the dielectric constants were about 77, 53 and 42, respectively, at room temperature, which are larger than our results [9]. In addition, Fennie et al. have investigated the dielectric properties of Sr_2TiO_4 using density-functional theory. As a theoretical result, the dielectric constant of Sr_2TiO_4 was 38, which is also larger than our result [21]. One possible reason for these results is that the sol–gel method needs complex reagents and several solvents, and these chemicals may introduce additional impurities and influence the dielectric properties.

The dielectric loss is a type of energy loss that manifests as the production of heat in an alternating electric field. The frequency dependency of the dielectric loss for the $Sr_{n+1}Ti_nO_{3n+1}$ series of samples in the 1 kHz to 10 MHz range are shown in Fig. 6(b). It can be seen that the dielectric loss decreases with the index n for fixed frequency. $SrTiO_3$ shows the largest dielectric loss where the value is in the range of 0.02–0.15. This value is similar to several reported results [10,22]. Sr_2TiO_4 has the smallest dielectric loss of the four samples, and it is less than 0.01. The four samples all show dielectric losses lower than 4×10^{-2} above 100 kHz. The dependence on the index n of the dielectric properties of the $Sr_{n+1}Ti_nO_{3n+1}$ ($n=1, 2, 3, \infty$) series has been analyzed above, and was found to vary regularly with their crystal structures.

4. Conclusion

In this paper, a series of high purity $Sr_{n+1}Ti_nO_{3n+1}$ ($n=1, 2, 3, \infty$) nanoscale powders have been made using the sol–gel method. The chemical reaction mechanism of the sintering process has been studied by TG-DSC analysis. This suggests that the final sintering temperatures of $SrTiO_3$, $Sr_4Ti_3O_{10}$, $Sr_3Ti_2O_7$ and Sr_2TiO_4 are 800 °C, 950 °C, 1050 °C and 1050 °C, respectively. XRD was used to carry out phase analysis and no impurity peaks appeared. From the FT-IR spectrum and Fourier transform Raman spectrum, it may be seen that the vibration peaks change regularly and become more and more similar to $SrTiO_3$ as the index n increases. The dielectric constant and dielectric loss show a gradually change with the index n. At 100 kHz, the dielectric constants of $SrTiO_3$, $Sr_4Ti_3O_{10}$, $Sr_3Ti_2O_7$ and Sr_2TiO_4 are 114, 55, 41 and 30, respectively. The dielectric constants of the four materials increase with increasing n. All the powders have dielectric losses lower than 4×10^{-2} above 100 kHz. Hence this type of powder has promising applications in the high frequency region.

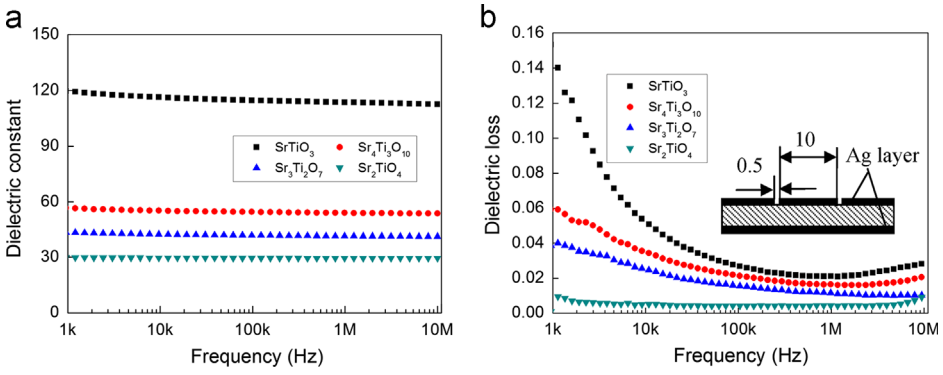

Fig. 6. Frequency dependence of (a) dielectric constants and (b) dielectric loss for $Sr_{n+1}Ti_nO_{3n+1}$ ($n=1, 2, 3, \infty$) samples. The inset of (b) is a schematic diagram of the device under test. The size unit in the inset is millimeters.

Acknowledgments

This work is supported by the Key Item Science Foundation of Hebei Province (Grant no. 10965125D) and the National Natural Science Foundation of China, under the Contract no. NSF-11174069.

References

[1] F.M. Pontes, E.J.H. Lee, E.R. Leite, E. Longo, High dielectric constant of $SrTiO_3$ thin films prepared by chemical process, Journal of Materials Science 35 (2000) 4783–4787.
[2] B. Bialobok, J. Trawczunski, T. Rzadki, W. Mista, M. Zawadzki, Catalytic combustion of soot over alkali doped $SrTiO_3$, Catalysis Today 119 (2007) 278–285.
[3] S.N. Ruddlesden, P. Popper, New compounds of the K_2NiF_4 type, Acta Crystallographica 10 (1957) 538–539.
[4] S.N. Ruddlesden, P. Popper, The compound $Sr_3Ti_2O_7$ and its structure, Acta Crystallographica 11 (1958) 54–55.
[5] J.H. Haeni, D.C. Theis, D.G. Schlom, H. Chang, I. Takeuchi, Epitaxial growth of the first five members of the $Sr_{n+1}Ti_nO_{3n+1}$ Ruddlesden–Popper homologous series, Applied Physics Letters 78 (2001) 3292–3294.
[6] G. Pfaff, Sol–gel synthesis of strontium titanate powders of various compositions, Journal of Material Chemistry 3 (7) (1993) 721–724.
[7] X.W. Wang, Z.Y. Zhang, S.X. Zhou, Preparation of nano-crystalline $SrTiO_3$ powder in sol–gel process, Materials Science and Engineering: B 86 (2001) 29–33.
[8] J.H. Sohn, Y. Inaguma, M. Itoh, T. Nakamura, Cooperative interaction of oxygen octahedra for dielectric properties in the perovskite-related layered compounds $Sr_{n+1}Ti_nO_{3n+1}$, $Ca_{n+1}Ti_nO_{3n+1}$ and $Sr_{n+1}(Ti_{0.5}Sn_{0.5})_nO_{3n+1}$ ($n=1$, 2, 3 and ∞), Materials Science and Engineering: B 41 (1996) 50–54.
[9] N.D. Orloff, W. Tian, C.J. Fennie, et al., Broadband dielectric spectroscopy of Ruddlesden–Popper $Sr_{n+1}Ti_nO_{3n+1}$ ($n=1$, 2, 3) thin films, Applied Physics Letters 94 (2009) 042908–042911.
[10] T. Ahmad, A.K. Ganguli, Reverse micellar route to nanocrystalline titanates ($SrTiO_3$, Sr_2TiO_4, and $PbTiO_3$): structural aspects and dielectric properties, Journal of the American Ceramic Society 89 (4) (2006) 1326–1332.
[11] R. Wurm, O. Dernovsek, P. Greil, Sol–gel derived $SrTiO_3$ and $SrZrO_3$ coatings on SiC and C-fibers, Journal of Materials Science 34 (1999) 4031–4037.
[12] S. Kamba, P. Samoukhina, F. Kadlec, et al., Composition dependence of the lattice vibrations in $Sr_{n+1}Ti_nO_{3n+1}$ Ruddlesden–Popper homologous series, Journal of the European Ceramic Society 23 (2003) 2639–2645.
[13] W.G. Nilsen, J.G. Skinner, Raman spectrum of strontium titanate, Journal of Chemical Physics 48 (1986) 2240–2249.
[14] Y.F. Gao, Y. Masuda, T. Yonezawa, K. Koumoto, Site-selective deposition and micropatterning of $SrTiO_3$ thin film on self-assembled monolayers by the liquid phase deposition method, Chemistry of Materials 14 (2002) 5006–5014.
[15] T. Sekine, K. Uchinokura, E. Matsuura, Raman scattering from two-phonon resonance states in $SrTiO_3$, Solid State Communications 18 (1976) 569–572.
[16] R. Ouillon, J.-P.P. Lucarre, P. Ranson, et al., A Raman scattering study of the phase transition in $SrTiO_3$ and in the mixed system $(Sr_{1-x}Ca_x)TiO_3$ at ambient pressure from $T=300$ K down to 8 K, Journal of Physics: Condensed Matter 14 (2002) 2079–2092.
[17] A.A. Sirenko, I.A. Akimov, J.R. Fox, A.M. Clark, et al., Observation of the first-order Raman scattering in $SrTiO_3$ thin films, Physical Review Letters 82 (1999) 4500–4503.
[18] J. Petzelt, T. Ostapchuk, I. Gregora, et al., Dielectric, infrared, and Raman response of undoped $SrTiO_3$ ceramics: evidence of polar grain boundaries, Physical Review B 64 (2001) 1184111.
[19] J.H. Jeon, Effect of $SrTiO_3$ concentration and sintering temperature on microstructure and dielectric constant of $Ba_{1-x}Sr_xTiO_3$, Journal of the European Ceramic Society 24 (2004) 1045–1048.
[20] P.L. Wise, I.M. Reaney, W.E. Lee, et al., Structure–microwave property relations in $(Sr_xCa_{(1x)})_{n+1}Ti_nO_{3n+1}$, Journal of the European Ceramic Society 21 (2001) 1723–1726.
[21] C.J. Fennie, K.M. Rabe, Structural and dielectric properties of Sr_2TiO_4 from first principles, Physical Review B 68 (2003) 184111.
[22] B.K. Choudhury, K.V. Rao, R.N.P. Choudhury, Dielectric properties of $SrTiO_3$ single crystals subjected to high electric fields and later irradiated with X-ray or γ-rays, Journal of Materials Science 24 (10) (1989) 3469–3474.